Accepted Manuscript

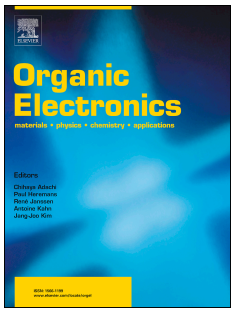

Flexible rewritable organic memory devices using nitrogen-doped CNTs/PEDOT:PSS composites

I. Rosales-Gallegos, J.A. Ávila-Niño, D. Hérnandez-Arriaga, M. Reyes-Reyes, R. López-Sandoval

PII: S1566-1199(17)30117-9

DOI: 10.1016/j.orgel.2017.03.014

Reference: ORGELE 4011

To appear in: *Organic Electronics*

Received Date: 30 December 2016

Revised Date: 8 March 2017

Accepted Date: 9 March 2017

Please cite this article as: I. Rosales-Gallegos, J.A. Ávila-Niño, D. Hérnandez-Arriaga, M. Reyes-Reyes, R. López-Sandoval, Flexible rewritable organic memory devices using nitrogen-doped CNTs/PEDOT:PSS composites, *Organic Electronics* (2017), doi: 10.1016/j.orgel.2017.03.014.

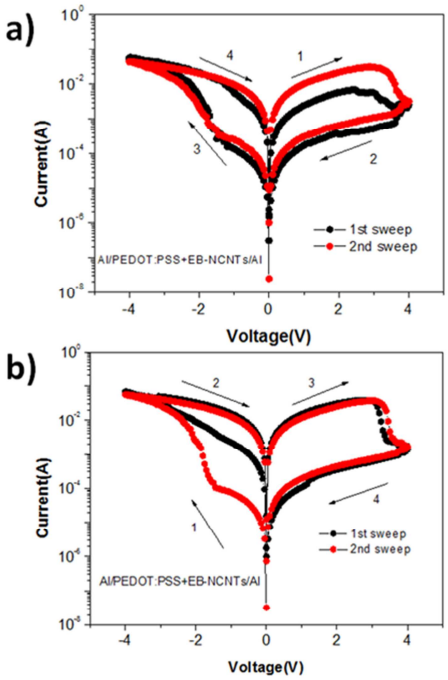

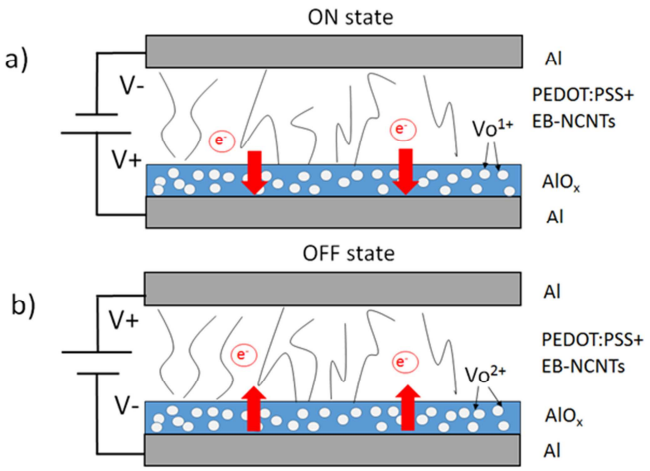

Flexible rewritable organic memory devices using nitrogen-doped CNTs/PEDOT:PSS composites

I. Rosales-Gallegos[1], J. A. Ávila-Niño[2], D. Hérnandez-Arriaga[1], M. Reyes-Reyes[1,*], R. López-Sandoval[2,*]

[1]Instituto de Investigación en Comunicación Óptica, Universidad Autónoma de San Luis Potosí, Álvaro Obregón 64, San Luis Potosí 78000, Mexico.

[2]Advanced Materials Department, IPICYT, Camino a la Presa San José 2055, Col. Lomas 4a sección, San Luis Potosí 78216, Mexico.

ABSTRACT

Nonvolatile rewritable organic memory devices based on poly(3,4-ethylene dioxythiophene):poly(styrenesulfonate) (PEDOT:PSS) and nitrogen doped multi-walled carbon nanotube (NCNT) nanocomposites were fabricated on glass and PET substrates. Organic memory devices with bistable resistive switching were obtained using very low NCTN concentration (~0.002 wt%) in the polymeric matrix. The memory devices exhibited a good ON/OFF ratio of approximately three orders of magnitude, a good retention time of 10^4 s under operating voltages ≤ |4V| and a few hundredths of write-read-erase-read cycles. The bistable resistive switching is mainly attributed to the creation of oxygen vacancies. These defects are introduced into the thin native Al oxide (AlOx) layer on the bottom electrode during the first voltage sweep. The well-dispersed NCNTs immersed in PEDOT:PSS play a key role as conductive channels for the electronic transport, hindering the electron trapping at the AlOx-polymer interface and inducing a soft dielectric breakdown of the AlOx layer. These PEDOT:PSS+NCNTs memory devices are to easy to apply in flexible low-cost technology and provide the possibility of large-scale integration.

INTRODUCTION

Currently, flexible electronics has become very attractive for the next generation of electronic devices, particularly wearable and foldable applications due to their bendable properties [1]. Non-volatile memory devices [2-7], field effect transistors [8,9], light-emitting diodes [10,11], logic circuits [12], static random access memories [13] and other devices using organic materials have been fabricated onto flexible substrates, allowing their application in large area electronics [14] and in the Internet of Things [15]. In particular, polyethylene terephthalate (PET) has been used as a substrate in various electronic applications because of its low cost, good thermal stability, excellent transparency in the visible range and good mechanical flexibility [2,3,5,7-9,16].

Among the various organic electronic devices, one of the most studied is the resistive memory [15,17,18]. Organic rewritable resistive memories consist of a polymer layer or a polymer composite sandwiched between two metal electrodes, which can be switched several times between two different conductive states using voltage pulses or voltage sweeps [19,20]. These organic resistive devices are becoming an alternative to the conventional memory technology due to the possibility of device miniaturization using scalable cross-bar array architecture, good operation speed and low energy consumption [15,17,18]. In addition, the fabrication of organic memories is easy and inexpensive, and the flexibility of the organic materials allows their deposition on either polymeric substrates or other unconventional substrates [2,5,7]. A variety of organic materials have been used for the fabrication of resistive organic memories [15,17,18], of which the most interesting are the carbon nanostructures [3,21-27]. In some cases, these carbon nanostructures, such as graphene oxide, reduced graphene oxide and graphene grown by CVD, are used as the resistive switching layer [3,21,22]. In other cases, these nanostructures are embedded in polymer matrices [23-27]. In some of these works the presence of native Al oxide layer (AlOx) is crucial for the resistive switching [18,20,22,27]. Nanocomposites of carbon nanostructures in a polymer matrix sandwiched between two metal electrodes have shown write-once-read-many (WORM) [23-25] and rewritable [26,27] memory behaviors. In particular, nanocomposites of the organic semiconducting polymer PEDOT:PSS and

carbon nanotubes (CNTs) have been used as the active layer in resistive organic memory devices [24,25,27].

One of the main disadvantages posed by the carbon nanostructures, such as CNTs, is the poor compatibility with polymer matrices, and therefore, it is difficult to obtain a homogeneous distribution of carbon nanostructures in the polymer [26, 28]. To improve the dispersion of the carbon nanostructures in the polymeric matrix, modification of their surface by anchoring functional groups via acid treatment is necessary [26]. However, these modifications of the nanostructure surfaces can cause undesired changes and deterioration in the properties of nanostructures [29]. Several methods to restore their graphitic properties, either partially or totally, and to remove the various defects and the oxygen functional groups have been implemented [11,28,29]. For the reduction of carbon nanostructures, some of these methods use a thermal treatment at high temperature in a mixture of gases, and some of these gases contain nitrogen [11,28]. It has been shown that the use of reducing agents containing nitrogen, in addition to restoring the graphitic properties, leads to nitrogen doping of carbon nanostructures [11,21,28]. This results in a change in the properties of the carbon nanostructures, such as an increase in their conductivity because of electron excess [28,30] and modification of their work function; both properties can be controlled as a function of the nitrogen doping concentration for their use in organic devices. Several works using nitrogen doped CNTs (NCNTs) embedded in a polymeric matrix for memory applications have been reported: Hwang et al. reported an Al/polystyrene and NCNT/Al rewritable memory [28], and Mamo et al. reported an Al/poly(vinyl phenol) and NCNT/Al WORM memory [30].

In the present work, Al/nitrogen doped multiwalled carbon nanotubes embedded in a PEDOT:PSS matrix/Al rewritable memory devices were fabricated. PEDOT:PSS as a polymeric matrix presents several advantages compared with other polymers, such as high conductivity and good processability. Additionally, PEDOT:PSS is provided by the supplier as an aqueous dispersion and, the use of a toxic solvent, such as chloroform or toluene, is not necessary for its deposition. Two types of N doped CNTs were synthesized using the same experimental configuration and used in organic memory devices: (a) NCNTs synthesized using benzylamine (B-NCNTs), as the carbon and nitrogen source and

ferrocene as a catalyst and (b) NCNTs synthesized using ethanol, as carbon source, mixed with benzylamine, as the carbon and nitrogen source (EB-NCNTs) and ferrocene as a catalyst. The use of an ethanol-benzylamine reaction mixture allows anchoring of oxygen functional groups on the EB-NCNTs surface without using an acid treatment, improving their solubility in the PEDOT:PSS matrix while not causing great damage on their graphene layers. In this way, the main goal of this work was to study the importance of obtaining a homogeneous dispersion of NCNTs in the PEDOT:PSS matrix and the role of the native Al oxide layer on the bottom electrode in reliable resistive switching of Al/PEDOT:PSS+NCNTs/Al memory devices.

EXPERIMENTAL

Poly(3,4-ethylenedioxythiophene):poly(styrenesulfonate), PEDOT:PSS (Clevios P), was purchased from Heraeus. Nitrogen doped multiwalled carbon nanotubes were synthesized by the spray pyrolysis method: (a) using only benzylamine as the carbon and nitrogen source [31] and (b) using a mix of ethanol and benzylamine (9:1 v/v) [32-34] as the carbon, nitrogen and oxygen source; in both types of synthesized samples, ferrocene was used as a catalyst. Before the deposition of the Al bottom electrode, the 1 in^2 Dow Corning glass or PET (Dupont Teijin Films) substrates were cleaned by washing them in acetone, methanol and isopropanol ultrasonic baths for 20 min and then dried for 40 min. After that, a 70 nm Al bottom electrode was deposited by thermal evaporation at 10^{-6} Torr and patterned using a shadow mask or conventional photolithographic process onto the glass or PET substrates. The photolithography process (Figure S1) was performed by depositing a thin film of a positive photoresist S1818 via spin coating. The deposited film was exposed to UV radiation by using a HYBRALIGN SERIES 200 lamp for 45 seconds through an ink mask printed on photographic paper. The exposed film was immersed in CD30 developer and finally waste developer was removed by washing the samples in deionized water. The nitrogen doped carbon nanotubes and PEDOT:PSS composites were prepared by using the following procedure: the carbon nanotubes were dissolved in isopropanol and the dispersion was ultrasonicated for 40 min at 58 °C. After that, 0.002 wt% of EB-NCNTs (or B-NCNTs) was mixed with the previously filtered PEDOT:PSS aqueous solution (1 µm pore size filter) for 150 min by ultrasonication at room temperature. This composite was

spin-coated at 2500 rpm for 40 seconds onto the Al bottom electrode and then dried at 100 °C for 15 min. The PEDOT:PSS+ NCNT film thickness was measured using a Tencor Alpha-Step 500 surface profiler and its thickness was approximately 80 nm. Finally, a thermally evaporated top electrode was deposited onto the polymeric composite layer and patterned using a shadow mask. The active area of the devices corresponds to the overlapping area between the bottom and top electrodes (Figure 1), which are 6 mm^2 and 0.1 mm^2 for shadow masks and conventional photolithography, respectively.

Current-voltage measurements were performed by a programmable Keithley 236 source meter at room conditions. In all the current-voltage measurements of the memory devices, the bias voltage is applied to the top electrode with the bottom electrode grounded. At least 90% of the fabricated memory devices showed good reproducibility. The roughness measurements and morphology images of films were determined using a Nanoscope Versaprobe 5 atomic force microscope in contact mode. The morphology of the synthesized NCNTs was analyzed with conventional transmission electron microscopy (TEM) by using a Philips TECNAI-F30 HRTEM transmission microscope operated at 300 kV. NCNT films for ATR-FTIR measurement were prepared by dispersing NCNTs (~1 mg) in isopropanol (~1 ml) using a sonication bath for 1 hour and the solution was immediately dropped on the surface of a piranha cleaned glass slide and then allowed to evaporate. The IR measurements were recorded on a NICOLET 6700 Thermo Scientific Instrument. Chemical analysis by XPS was performed using a Physical Electronics Ulvac Phi Versa Probe II spectrometer employing an Al Kα X-ray source operated at 15 kV and 25W with a take-off angle of 45° and typical operating pressures at ~1×10^{-9} Torr.

RESULTS

Figure 2 shows typical (a) TEM image and (b) FTIR spectra of synthesized nitrogen doped CNTs. The TEM image shows the two typical types of nitrogen doped CNT morphologies reported in the literature, the bamboo-like and multi-compartment walls. The most predominant morphology in the synthesized sample was the bamboo-like structure [31]. The FTIR spectra in Figure 2b show peaks at 2974 cm^{-1} and 2900 cm^{-1}, assigned to the presence of C-H stretching modes [33,35-38]. The FTIR spectra also show three IR bands at ~1515 cm^{-1}, ~1230 cm^{-1} and ~1050 cm^{-1} associated with C=N and C-N stretching modes

[39-41]. The IR bands at 1515 cm^{-1} (C=N) and 1230 cm^{-1} (C-N) are evidence of the nitrogen incorporation into the graphitic network, whereas the IR band at 1050 cm^{-1} comes from C-N bonds not in the graphene layer, i.e., amine-like C-N bonds. The main differences observed in the FTIR spectra for both types of samples are as follows: (a) the IR spectrum of the B-NCNT sample clearly shows the presence of C-H bonds on its surface, and (b) there is a slight shift of the IR bands for the C-N and C=N bonds between both types of NCNTs. These differences in the IR spectra are related to high nitrogen doping on the B-NCNT surface, i.e., a great quantity of defects on the graphitic layers. On the other hand, the presence of oxygen atoms coming from the ethanol decomposition during the synthesis of EB-NCNTs results in the incorporation of oxygen functional groups on their surfaces.

A dispersion stability study of carbon nanotubes doped with different percentages of nitrogen in a variety of solvents has been reported in literature [42]. It was shown that nanotubes doped with nitrogen atoms can form stable dispersions in solvents with surface energies between 66 mJ/m^2 and 72 mJ/m^2. Furthermore, 82% of the initial concentration of CNTs with a high nitrogen doping remain well diluted in dimetylacetamide, which has a surface energy of 66 mJ/m^2. This high dilution of NCNTs occurs in solvents with a surface energy very close to that of the NCNTs because the interaction between the nanomaterial surface and the solvent is strong enough to compensate for the solvation and nanomaterial exfoliation. When solvents with very different surface energy than that of NCNTs are used, the amount of dispersed NCNTs decreases abruptly. For example, it was shown that at most 0.5% of the initial concentration of NCNTs can be diluted in isopropanol, which has a surface energy of 51 mJ/m^2. To study the effect of the use of ethanol in the reaction mixture on the surface functionalization of the NCNTs, we performed solubility tests of the two types of synthesized NCNTs. To perform the solubility test, 1 mg of the two kinds of synthesized carbon nanotubes, EB-NCNTs and B-NCNTs, was placed in vials containing 3 ml of isopropanol. Samples were sonicated for 30 min using an ultrasonic bath at 42 kHz. The result of this process is shown in Figure 2c; EB-NCNTs remain well dispersed in the liquid medium, even after 24 hours, while B-NCNTs are aggregated and completely sedimented 30 min after sonication. This implies that the use of an ethanol-benzylamine

reaction mixture modifies the surface energy of the synthesized nanotubes, allowing the formation of stable dispersions in isopropanol.

Good homogeneous dispersion of CNTs in liquid medium is essential for the fabrication of nanocomposites used as the active layer in various organic devices such as organic resistive memories. On the other hand, PEDOT:PSS is a polymer in aqueous dispersion and can be easily mixed in hydrophilic solvents, allowing a more homogeneous mixture of EB-NCNTs with PEDOT:PSS and, therefore, nanocomposite films with good quality can be obtained. Figure S2 shows the morphological characterization by topographic atomic force microscopy of pristine PEDOT:PSS (Figure S2a) and PEDOT:PSS+EB-NCNT (Figure S2b) films; these films present only a slight difference in average roughness, 0.9 nm and 0.6 nm for PEDOT:PSS and PEDOT:PSS+EB-NCNT films, respectively. Furthermore, the nitrogen content on the graphitic layers and its effect on the surface chemistry of CNTs can be analyzed using XPS [43-45]. XPS measurements of EB-NCNTs presented an atomic nitrogen concentration of approximately 1%, while B-NCNTs showed an atomic nitrogen concentration of approximately 3.5%. Figure 3a shows the C1s spectra of these nanotubes with different nitrogen contents. From this figure, we observe that the position of the C1s main peak at 284.4 eV shifts to 284.6 eV as a function of the atomic nitrogen concentration on the nanotubes. This peak shift has been related to an increase in structural disorder, i.e., a disruption of the structure graphiticity due to the incorporation of nitrogen atoms into the graphitic lattice [44,45]. In addition, the deconvolution of the C1s XPS spectrum shows bands near 285.1 ± 0.1 and 286.2 ± 0.1 eV (Figure 3a and S3), which have been assigned to different types of N-C bonds and show intensity changes as a function of the atomic nitrogen concentration on the NCNTs [43,44]. High N1s resolution spectra (Figure 3b) from both types of NCNTs show that while the spectrum of B-NCNTs presents four bands clearly defined at 398.5 eV, 401 eV, 404 eV and 405 eV, the bands of EB-NCNTs are not well defined and are more difficult to observe. These bands have been assigned to pyridinic nitrogen (398.5 eV), quaternary nitrogen (401 eV), intercalated nitrogen molecules (404 eV) and nitrogen oxide species (405 eV) [44,45]. Thus, the XPS measurements show differences in the surface chemistry of both nanostructures, which are responsible for their different solubilities in isopropanol.

Six different types of devices were fabricated. The first ones are using only PEDOT:PSS film (device A) and using B-NCNT immersed in PEDOT:PSS film (device B) as the active layer, both devices deposited on glass substrates and thermally deposited Al bottom electrodes. The next devices were fabricated using PEDOT:PSS+EB-NCNTs as the active layer and thermally deposited Al bottom electrode with the following configuration: glass/Al/active-layer/Al (device C) and PET/Al/active-layer/Al (device D). In the last two devices, with the configurations glass/Al/active-layer/Al (device E) and PET/Al/active-layer/Al (device F), a patterning of the bottom electrode using a photolithography process was performed to reduce by approximately sixty times the active area compared with those obtained using a shadow mask. The I-V electrical characterization of these devices is shown in Figure 4. In all cases, the voltage was swept from 0 to 4 V, from 4 to -4 V and from -4 to 0 V without previous electroforming. As shown in Figure 4, the device without nanotubes (device A) or those fabricated using B-NCNTs immersed in the PEDOT:PSS matrix (device B) do not show a memory behavior, whereas all the devices with EB-NCNTs (devices C, D, E and F) embedded in a PEDOT:PSS layer show a bistable memory behavior. Device A presents an electrical behavior similar to that discussed in our previous work [27] and device B shows a slight increase of current flow through the device around -3 V due to the presence of nitrogen doped carbon nanotubes in the active layer. However, as the dispersion of these kinds of CNTs was not reliable in comparison with those fabricated with EB-NCNTs (Figure 4b), devices B (Figure 4a) presented an erratic electrical behavior, i.e., it was not reproducible. In the case of the devices with EB-NCNTs (devices C, D, E and F), the write process is performed at approximately -2 V switching from the OFF state to the ON state and these devices can be erased at approximately 3 V switching from the ON state to the OFF state. These devices presented only minor variations in their electrical behavior. The results indicate that the presence of conductive CNTs immersed in the polymeric matrix is necessary to provide load transfer across the CNT/matrix interface. Furthermore to obtain the electrical bistability in the memory devices, the CNTs must be very well dispersed in the PEDOT:PSS films, forming conductive pathways that control the flux of charge between both electrodes.

On the other hand, the EB-NCNTs concentration (0.002 wt%) embedded in PEDOT:PSS is very small, but these nitrogen doped carbon nanostructures abruptly

changed the electrical properties of the memory devices. It has been shown that when very small CNT concentrations (< 0.2 wt%) are embedded in insulating polymeric matrices, the electrical properties of the resulting devices are those of the insulating hosts [46,47]. Thus, the differences in the electrical behavior compared with our devices could be related to the fact that PEDOT: PSS is a p-type semiconducting polymer and the presence of the electron-rich EB-NCNTs in the PEDOT:PSS matrix enhances the charge transport through the device. Furthermore, these works showed [46,47] that the CNT concentration embedded in the insulator polymeric matrix can modulate the electrical response of the devices, i.e., the same device configuration can show WORM (~1 wt% CNTs), rewritable (~2 wt% CNTs) or ohmic (> 3 wt% CNTs) behavior depending of the CNT concentration embedded in the polymeric matrix. In addition, the role of N-doped CNTs (~ 1.5 wt%) in rewritable polymeric matrices has been reported in the literature. These electron rich N-doped CNTs create shallow charge traps [28] compared to pristine ones, and this tuning of charge traps can be used for the fabrication of multi-level resistive memories. In all these cases, however, it is proposed that the mechanism of the rewritable memory behavior is related to a charge carrier trapping/detrapping process occurring in the CNT network. For CNT concentrations of approximately 1.5 wt%, the nanostructures make contact with both electrodes. The energy differences between the work functions of the CNTs (~5.1 eV) and the electrodes of the organic memories, generally Al (~4.3 eV), prevent the trapped charges in CNTs from being released when the power supply is turned off, resulting in nonvolatile memory behavior. Under the application of a bias voltage with reverse polarity and reliable magnitude, the trapped charges in the CNTs will be neutralized or extracted, and therefore, the device will be returned to its low conductivity state. Thus, this mechanism cannot describe the switching behavior of our memories, where the CNT concentrations in our devices are almost three orders of magnitude below those reported in the literature for the mechanism of a charge carrier trapping/detrapping process in CNTs networks.

A possible mechanism for the electrical bistability and bipolar switching in our memory devices could be related to the presence of a native oxide layer at the Al/polymeric nanocomposite interface, as discussed in our previous report, where the use of an Al electrode is needed to obtain a rewritable memory [27]. The application of an electroforming voltage could induce the creation of oxygen vacancies (V_O) in the oxide

layer of Al [48]. In this way, this switching mechanism could be related to the electronic barrier changes at the Al/AlOx interface caused by the drift of oxygen vacancies or oxygen ions under the application of opposite electric fields. The vacancy drift toward the interface creates conductive pathways switching the electronic barrier to the ON state; applying the opposite polarity will cause a drift of vacancies away from the interface, changing the interface to the OFF state [48,49]. This mechanism was used to explain the electrical switching in Al/TiO_2/Al memory devices, where it was shown, by energy-filtered–transmission electron microscopy, that the drift of oxygen ions at the interface between the Al top electrode and the bulk TiO_2 region during the ON-OFF switching is the responsible mechanism for the bipolar resistive switching [50].

Al/graphene oxide (GO) film/Al devices presented a similar bipolar resistive switching behavior, which was attributed to the rupture and formation of conducting filaments, due to oxygen ion drifts at the top interface [22]. In Al/GO film/Al devices, it was shown that the UV ozone-treated native AlOx layer at the bottom electrode mainly protects the devices from an irreversible dielectric breakdown, but using Au as a bottom electrode generates this breakdown [22]. However in our devices, we consider that the native AlOx layer on the Al bottom electrode causes the bistable resistive switching. When a positive bias voltage is applied to the top electrode, during the first voltage sweep, the density of oxygen vacancies, V_O^{2+} (electron empty oxygen vacancies V_O), created and localized in the native oxide layer AlOx on the bottom electrode is increased due to the migration of oxygen ions (O^{2-}) to the top electrode. As a consequence the device switches to the high resistance state, i.e., the device is electroformed in the OFF state [48]. If instead, a negative bias voltage is applied to the top electrode in the first voltage sweep, a similar process occurs in the AlOx layer on the bottom electrode, and the device is electroformed in the ON state; the resistive switching of the memory device is basically the same (Figure S4). Additionally, we observed that a previous process of electrical forming in the devices was unnecessary for showing a memory type behavior. This is related to the presence of a native Al oxide layer on the bottom electrode, which is extremely thin, between 2 and 4 nm. It has been shown in devices based on metal oxides that the electroforming process can be eliminated using a very thin metal oxide layer of a few nanometers, alone or in combination with a conductive oxide layer [48], which corresponds well with our results.

To corroborate the assumption that the existence of AlOx on the bottom electrode is responsible for the memory behavior, we used gold as an electrode, a material difficult to oxidize, in different configurations of the memory device. At first, a device fabricated with a Au film as the bottom electrode, in the Au/PEDOT:PSS+EB-NCNT /Al configuration, showed no memory behavior (Figure 5a). When a Au film was used as the top electrode, these Al/AlOx/PEDOT:PSS+EB-NCNT/Au devices showed rewritable behavior (Figure 5b, Figure S5). These last results were almost the same as those previously obtained (Figure 4b, Figure S4), indicating that much of this behavior can be related to the bottom electrode. On the other hand, I-V curves from Al/AlOx/PEDOT:PSS+EB-NCNT/Al (Figure 6a) and Al/AlOx/PEDOT:PSS+EB-NCNT/Au (Figure 6b) devices were plotted using log-log plots to identify the transport mechanism through the devices. The slopes of the log I-log V curves from the OFF state showed a slope change from m = 1 to 2. This behavior is consistent with shallow traps associated with a space charge limited current (SCLC) transport mechanism. The ON state presented an ohmic behavior with m ≈ 1, which shows the formation of conductive filaments; however, these are not metallic filaments because they exhibited a resistance of a few hundred ohms [51,52]. Note that in the memory devices where the resistive switching involves the drift of oxygen vacancies or oxygen ions, the ON states do not exhibit ohmic behavior [22, 48-50]. Moreover, during the oxygen vacancy creation process, the O^{2-} ions drift toward the anode evolve into O_2 gas and escape from the memory device. Therefore, it is unlikely that by changing the voltage polarity, these O^{2-} ions can be reintroduced into the AlOx layer and cause the resistive switching. Contrary to what was reported by Yang et al. [48] in their study of Pt/TiO_2/Pt memory devices, the bubbles created in our devices are permanent and neither disappear nor shrink as a function of voltage polarity (see Figure S6).

On the other hand, in some resistive memory devices where an AlOx layer is used as the resistive switching layer, the mechanism responsible for the resistive switching is the creation (destruction) of a sub-band, a mid-gap band, due to the change of V_O^{2+} (electron empty oxygen vacancies V_O) to V_O^{1+} (electron occupied V_O) by an electron injection (ejection) [51,52]. These memory devices exhibit an ohmic ON state. Based on the above discussion, we propose that the origin of the bistable resistive switching in our devices is the creation/destruction of a sub-band caused by an increase/decrease of the number of

electrons in the oxygen vacancies located in the AlOx layer of the bottom electrode (Figure 7) and not in the creation/destruction of conductive filaments due to the movement of O ions. However, in our memory devices, the native AlOx layer thickness is between 2 and 4 nm, while the thickness of the PEDOT:PSS + EB-NCNTs nanocomposite is approximately 80 nm. Thus, the EB-NCNTs embedded in the polymeric matrix and the sub-band formation in the AlOx layer are important for the electrical bistability and bipolar resistive switching. If EB-NCNTs are not embedded in the polymeric matrix, the devices do not show memory-like behavior. EB-NCNTs are conductive channels for electronic transport that reduce electron trapping at the AlOx polymer film interface, which induces a soft dielectric breakdown in the AlOx layer. In addition, it is very important that the CNTs are well dispersed in the polymer matrix and that the graphitic layers are doped with low concentrations of N atoms (~ 1% at). The effect of nitrogen doping, based on the absence of electrical forming in our devices, could be related to interactions between the nitrogen atoms on the graphitic layers and the AlOx native layer, where it has been shown that nitrogen doping of AlOx layers results in electroforming-free resistive memory devices [53].

The retention characteristics of the conductive states are also an important feature for memory devices. Figure 8 shows that the ON and OFF states read at 1 V were retained for at least 10^4 s with an ON/OFF ratio of three orders of magnitude, indicating a reasonably stable behavior in terms of information storage capability. For obtaining the write-read-erase-read (WRER) cycles, ON and OFF states were read by applying a 1 V pulse. The erasing process was performed by applying a 4 V pulse, switching the device from the ON state to the OFF state, whereas the writing process was performed by applying a -4 V pulse, switching from the OFF state to the ON state. The devices with thermally evaporated Al bottom electrodes showed 500 WRER cycles on glass substrate (device C) and 250 WRER cycles on the plastic substrate (device D). On the other hand, the devices for which a photolithography process was used for bottom electrode patterning onto glass (device E) and PET (device F) showed 200 and 100 cycles, respectively (Figure 9). Note that the memory devices on PET (devices D and F) showed good amount of WRER cycles without any additional process to improve the adhesion between the plastic substrate and the metal layer. The difference in the memory performances of the devices deposited on

different substrates using a shadow mask, those with an active area of 6 mm^2, is mainly related to the increase of the Al bottom electrode average roughness on PET compared with glass. In contrast to devices deposited on different substrates, when the Al bottom electrode is patterned using conventional photolithography, the decrease of WRER cycles is mainly due to the use of solvents during the photolithography process, which strongly affect the Al bottom electrode on the plastic substrate. As reported in the literature, oxygen-containing plastic substrates can oxidize the metal bottom electrode during deposition of metal and affect the electrical characteristics of the resistive memory [2]. Analysis of the Al bottom electrodes for the samples on glass and PET showed clear differences in the quality and average roughness of the electrodes (Figure S7). For the electrodes deposited on glass using a shadow mask, the average roughness is ~3.9 nm, while the electrodes patterned using conventional photolithography onto PET substrates present an average roughness of ~6.7 nm. Moreover, the inset in Figure S7 shows micrographs obtained by an optical microscope, where it is observed that the quality of the Al bottom electrode on the PET substrate is poor. However, these devices exhibited rewritable memory behavior indicating that the memory device size can be reduced without losing its memory device characteristics.

CONCLUSIONS

In resume, two types of nitrogen doped multiwalled CNTs were used in the fabrication of Al/PEDOT:PSS+ NCNT/Al organic memory devices onto glass and PET substrates. The first type of nitrogen doped CNTs was synthetized using benzylamine as a carbon and nitrogen source (B-NCNTs) whereas the second type was synthesized using an ethanol:benzylamine (9:1 v/v) mixture (EB-NCNTs) as a carbon and nitrogen source. The memories fabricated with EB-NCNTs showed rewritable memory behavior, whereas those fabricated with B-NCNTs showed no memory behavior. The difference in the electric responses between both memory devices is related to a better solubility of EB-NCNTs in isopropanol, which results in more a homogenous dispersion of these carbon nanotubes in the PEDOT:PSS matrix. Furthermore, the reversible resistive switching behavior of the devices fabricated with EB-NCNTs is mainly related to the formation of a native AlOx thin film (between 2 and 4 nm) on the bottom electrode and the creation of oxygen vacancies

(V_O) in the AlOx layer during the first voltage sweep. In addition, no electrical forming is necessary in these devices to produce memory type behavior, which is also related to the extremely thin native AlOx layer on the bottom electrode. Based on the I-V curve fits of the ON and OFF states, we propose that the resistive switching between both states is primarily due to the creation (destruction) of a sub-band in the electronic bandgap of the AlOx layer because of a change of V_O^{2+} (V_O^{1+}) to V_O^{1+} (V_O^{2+}) by electron injection (ejection). Additionally, the presence of the EB-NCNTs in the PEDOT:PSS matrix is necessary for the observed electrical bistability because EB-NCNTs are conductive channels for the electronic transport, hindering the electron trapping at the AlOx polymer film interface, which allows a soft dielectric breakdown in the AlOx layer. Finally, the retention characteristics of the glass/Al/PEDOT:PSS+EB-NCNT/Al and PET/Al/PEDOT:PSS+ EB-NCNT/Al devices, for both active areas, 6 and 0.1 mm^2, indicated a reasonably stable behavior in terms of information storage capability.

Acknowledgments

The authors acknowledge Francisco Ramírez Jacobo, M. Sc. Claudia G. Elías Alfaro, M. Sc. Dulce Partida-Gutierrez, M. Sc. Beatriz A. Rivera, Dr. Gladis Labrada and Dr. Hector G. Silva-Pereyra for technical assistance as well as to LINAN at IPICyT for providing access to its facilities. In addition, we thank Bob Rustin (Dupont USA) for providing us the PET substrates. X-ray photoelectron spectra were obtained by Dr. Mariela Bravo-Sanchez at LINAN-IPICYT. This work was supported by CONACYT through grant No. CB-2015-01-256484 (R.L.S) and research scholarship (I.A.R.G). J.A.A.N. thanks to the Fondo Sectorial-CONACYT-SENER-Hidrocarburos for a posdoctoral grant (2137).

Figure Captions

Figure 1. a) General diagram and b) photograph of the memory device using photolithography for bottom electrode patterning.

Figure 2. a) TEM image, b) FTIR spectra of nitrogen doped CNTs and (c) photograph of B-NCNTs and EB-NCNTs mixed with isopropanol sonicated for 30 min in a sonication bath.

Figure 3. a) C1s and b) N1s XPS spectra of NCNTs synthetized using ethanol:benzylamine mix 9:1 v/v (EB-NCNTs) and only benzylamine (B-NCNTs).

Figure 4. I-V characteristics of a) Al/PEDOT:PSS/Al and Al/PEDOT:PSS+B-NCNT/Al memories (A and B devices) and b) Al/PEDOT:PSS+EB-NCNT/Al memories (C,D,E and F devices).

Figure 5. I-V characteristics of a) Au/PEDOT:PSS+EB-NCNT/Al and b) Al/PEDOT:PSS+EB-NCNT/Au devices.

Figure 6. Log(I) vs log(V) curves for a) Al/PEDOT:PSS+EB-NCNT/Al and b) Al/ PEDOT:PSS+EB-NCNTs /Au devices.

Figure 7. Schematic representation of the mechanism of the memory devices. The diagrams showed the presence of oxygen vacancies in the native Al oxide film. a) Those traps are reduced to form a V_O^{1+} sub-band or conductive state due to the application of a negative voltage sweep to the top electrode. b) The traps are oxidized by the application of opposite polarity voltage sweeps forming a non-conducting state or OFF state.

Figure 8. Retention characteristics of Al/ PEDOT:PSS+EB-NCNTs /Al devices fabricated onto glass and PET substrates.

Figure 9. Write-read-erase-read curves of Al/PEDOT:PSS+EB-NCNT/Al memory devices on the glass substrate (C and E) and on the PET substrate (D and F).

REFERENCES

[1] R.H. Kim, H.J. Kim, I. Bae, S.K. Hwang, D.B. Velusamy, S.M. Cho, K. Takaishi, T. Muto, D. Hashizume, M. Uchimaya, P. Andre, F. Mathevet, B. Heinrich, T. Aoyama, D.E. Kim, H. Lee, J.C. Ribierre, C. Park, Non-volatile organic memory with sub-millimetre bending radius, Nat. Commun. 5 (2014) 3583.

[2] Y. Ji, B. Cho, S. Song, T.W. Kim, M. Choe, Y.H. Kahng, T.Lee, Stable switching characteristics of organic nonvolatile memory on a bent flexible substrate, Adv. Mater. 22 (2010) 3071-3075.

[3] D.I. Son, T.W. Kim, J.H. Shim, J.H. Jung, D.U. Lee, J.M. Lee, W.I. Park, W.K. Choi, Flexible organic bistable devices based on graphene embedded in an insulating poly(methyl methacrylate) polymer layer, Nano. Lett. 10 (2010) 2441-2447.

[4] S. Kim, H.Y. Jeong, S.K. Kim, S.Y. Choi, K.J. Lee, Flexible memristive memory array on plastic substrates, Nano Lett. (2011), 11, 5438-5442.

[5] Y.C. Lai, Y.X. Wang, Y.C. Huang, T.Y. Lin, Y.P. Hsieh, Y.J. Yang, Y.F. Chen, Rewritable, moldable and flexible sticker-type organic memory in arbitrary substrates, Adv. Funct. Mater. 24 (2014) 1430-1438.

[6] H.J. Yen, H. Tsai, C.Y. Kuo, W. Nie, A.D. Mohite, G. Gupta, J. Wang, J.H. Wu, G.S. Liou, H.L. Wang, Flexible memory devices with tunable electrical bistability via controlled energetics in donor-donor and donor-acceptor conjugated polymers, J.Mater.Chem. C 2 (2014) 4374-4378.

[7] B.H. Lee, H. Bae, H. Seong, D.I. Lee, H. Park, Y.J. Choi, S.G. Im, S.O. Kim, Y.K. Choi, Direct observation of carbon filament in water-resistant organic memory, ACS Nano 9 (2015) 7306-7313.

[8] U. Zschieschang, R. Hofmockel. R. Rodel, U. Kraft, M.J. Kang, K. Takimiya, T. Zaki, F. Letzkus, J. Butschke, H. Richter, J.N. Burghartz, H. Klauk, Megahertz operation of flexible low-voltage organic thin-film transistors, Org. Electron. 14 (2013) 1516-1520.

[9] S.K. Lee, H.Y. Jang, S. Jang, E. Choi, B.H. Hong, J. Lee, S. Park, J.H. Ahn, All graphene-based thin film transistors on flexible plastic substrates, Nano Lett. 12 (2012) 3472-3476.

[10] M.P. Gaj, A. Wei, C. Fuentes-Hernandez, Y. Zhang, R. Reit, W. Voit, S.R. Marder, B. Kippelen, Organic light-emitting diodes on shape memory polymer substrates for wereable electronics, Org. Electron. 25 (2015) 151-155.

[11] J.O. Hwang, J.S. Park, D.S. Choi, J.Y. Kim, S.H. Lee, K.E. Lee, Y.H. Kim, M.H. Song, S. Yoo, S.O. Kim, Workfuntion-tunable, N-doped reduced graphene transparent electrodes for high-performance polymer light-emitting diodes, ACS Nano 6 (2012) 159-167.

[12] H. Wang, P. Wei, Y. Li, J. Han, H.R. Lee, B.D. Naab, N. Liu, C. Wang, E. Adijanto, B.C.K. Tee, S. Morishita, Q. Li, Y. Gao, Y. Ciu, Z. Bao, Tuning the threshold voltage of carbon nanotube transistors by N-type molecular doping for robust and flexible complementary circuits, Proc. Natl. Acad. Sci. 111 (2014) 4776-4781.

[13] J.A. Avila-Niño, E.R. Patchett, D.M. Taylor, H.E. Assender, S.G. Yeates, Z. Ding, J.J. Morrison, Stable organic static random access memory from a roll-to-roll compatible vacuum evaporation, Org. Electron. 31 (2016) 77-81.

[14] D.M. Taylor, Vacuum-thermal-evaporation: the route for roll-to-roll production of large-area organic electronic circuits, Semicond. Sci. Technol. 30 (2015) 054002.

[15] M.T. Ghoneim, M.M. Hussain, Review on physically flexible non-volatile memory for internet of everything electronics, Electronics 4 (2015) 424-479.

[16] Y.H. Kim, C. Sachse, M.L. Machala, C. May, L. Muller-Meskamp, K. Leo, Highly conductive PEDOT:PSS electrode with optimized solvent and thermal post-treatment for ITO-free organic solar cells, Adv. Funct. Mater. 21 (2011) 1076-1081.

[17] J.C. Scott, D. Bozano, Nonvolatile memory elements based on organic materials, Adv. Mater. 19 (2007) 1452-1463.

[18] F. Pan, S. Gao, C. Chen, C. Song, F. Zeng, Recent progress in resistive random access memories: materials, switching mechanisms and performance, Mat. Sci. Eng. R 83 (2014) 1-59.

[19] T. Lee, Y. Chen, Organic resistive nonvolatile memory materials, MRS Bulletin 37 (2012) 144-149.

[20] F. Verbakel, S.C. Meskers, R.A. Janssen, H.L. Gomes, M. Colle, M. Buchel, D.M. de Leeuw, Reproducible resistive switching in nonvolatile organic memories, Appl. Phys. Lett. 91 (2007) 192103.

[21] S. Seo, Y. Yoon, J. Lee, Y. Park, H. Lee, Nitrogen-doped partially reduced graphene oxide rewritable nonvolatile memory, ACS Nano 7 (2013) 3607-3615.

[22] H.Y. Jeong, J.Y. Kim, J.W. Kim, J.O. Hwang, J.E. Kim, J.Y. Lee, T.H. Yoon, B.J. Cho, S.O. Kim, R.S. Ruoff, S.Y. Choi, Graphene oxide thin films for flexible nonvolatile memory applications, Nano Lett. 10 (2010) 4381-4386.

[23] I.A. Hummelgen, N.J. Coville, I. Cruz-Cruz, R. Rodrigues, Carbon nanostructures in organic WORM memory devices, J. Mater. Chem. C 2 (2014) 7708-7714.

[24] J.A. Avila-Niño, E. Segura-Cardenas, A.O. Sustaita, I. Cruz-Cruz, R. Lopez-Sandoval, M. Reyes-Reyes, Nonvolatile write-once-read-many-times memory device with functionalized-nanoshells/PEDOT:PSS nanocomposites, Mater. Sci. Eng. B 176 (2011) 462-466.

[25] Y. Sun, L. Li, D. Wen, X. Bai, G. Li, Bistable electrical switching and nonvolatile memory effect in carbon nanotube-poly(3,4-Ethylenedioxythiophene): poly(styrenesulfonate) composite films, Phys. Chem. Chem. Phys. 17 (2015) 17150-17158.

[26] G. Liu, Q.D. Ling, E.Y.H. Teo, C.X. Zhu, D.S.H. Chan, K.G. Neoh, E.T. Kang, Electrical conductance tuning and bistable switching in poly(N-vinylcarbazole)- carbon nanotube composite films, ACS Nano 3 (2009) 1929-1937.

[27] J.A. Avila-Niño, W.S. Machado, A.O. Sustaita, E. Segura-Cardenas, M. Reyes-Reyes, R. Lopez-Sandoval, I.A. Hummelgen, Organic low voltage rewritable memory device based on PEDOT:PSS/f-MWCNTs thin film, Org. Electron. 13 (2012) 2582-2588.

[28] S.K. Hwang, J.M. Lee, S. Kim, J.S. Park, H.I. Park, C.W. Ahn, K.J. Lee, T. Lee, S.O. Kim, Flexible multilevel resistive memory with controlled charge trap B- and N- doped carbon nanotubes, Nano Lett. 12 (2012) 2217-2221.

[29] S. Stankovich, D.A. Dikin, R.D. Piner, K.A. Kohlhaas, A. Kleinhammes, A. Jia, Y. Wu, S.T. Nguyen, R.S. Rouff, Synthesis of graphene-based nanosheets via chemical reduction of exfoliated graphite oxide, Carbon 45 (2007) 1558-1565.

[30] M.A. Mamo, A.O. Sustaita, Z.N. Tetana, N.J. Coville, I.A. Hummelgen, Nitrogen-doped, boron-doped and undoped multiwalled carbon nanotube/polymer composites in WORM memory devices, Nanotechnology 24 (2013) 125203.

[31] M. Reyes-Reyes, N. Grobert, R. Kamalakaran, T. Seeger, D. Golber, M. Ruhle, Y. Bando, H. Terrones, M. Terrones, Efficient encapsulation of gaseous nitrogen inside carbon nanotubes with bamboo-like structure using aerosol thermolysis, Chem. Phys. Lett. 396 (1-3) (2004) 167-173.

[32] A. Antal, A.A. Koos, F. Dillon, R.J. Nicholls, L. Bulusheva, N. Grobert, N-SWCNTs production by aerosol-assisted CVD method, Chem. Phys. Lett. 538 (2012) 108-111.

[33] E. Segura-Cardenas, M. Reyes-Reyes, R. Lopez-Sandoval, Effects of varying the content of alcohol in the reaction mixture on the graphitization of MWCNT and their surface functionalization, J. Phys. Chem. C 116 (17) (2012) 9783-9792.

[34] E. Segura-Cardenas, R. Lopez-Sandoval, D. Hernandez-Arriaga, J. Percino, V.M. Chapela, M. Reyes-Reyes, Oxygen to carbon atoms ratio effect on the size, morphology and purity of functionalized carbon nanoshells by using mixtures as carbon source, Carbon 76 (2014) 292-300.

[35] W. Li, Y. Bai, Y. Zhang, M. Sun, R. Cheng, X. Xu, W. Chen, Y. Mo, Effect of hydroxyl radical on the structure of multi-walled carbon nanotubes, Synth. Met. 155(3) (2005) 509-515.

[36] L. Zhang, V.U. Kiny, H. Peng, J. Zhu, R.F.M. Lobo, J.L. Margrave, V.N. Khabashesku, Sidewall functionalization of a single-walled carbon nanotubes with hydroxyl group-terminated moieties, Chem. Mater. 16(11) (2004) 2055-2061.

[37] R. Verdejo, S. Lamoriniere, B. Cottam, A. Bismarck, M. Shaffer, Removal of oxidation debries from multi-walled carbon nanotubes, Chem. Commun. 5 (2007) 513-515.

[38] P. Cañete-Rosales, V. Ortega, A. Alvarez-lueje, S. Bollo, M. Gonzalez, A. Anson, M.T. Martinez, Influence of size and oxidative treatments of multi-walled carbon nanotubes on their electrocatalytic properties, Electrochim. Acta 62 (2012) 163-171.

[39] M. Tabbal, P. Merel, S. Moisa, M. Chaker, E. Gat, A. Ricard, M. Moisan, S. Gujrathi, XPS and FTIR analysis of nitrogen incorporation in CNx thin films, Surf. Coat. Technol. 98 (1998) 1092-1096.

[40] Y.K. Yap, S. Kida, T. Aoyama, Y. Mori, T. Sasaki, Influence of negative DC bias voltage on structural transformation of carbon nitride at 600°C, Appl. Phys. Lett. 73 (1998) 915-917.

[41] S.H. Lai, Y.L. Chen, L.H. Chan, Y.M. Pan, X.W. Liu, H.C. Shih, The crystalline properties of carbon nitride nanotubes synthesized by electron cyclotron resonance plasma, Thin Solid Films 444 (2003) 38-43.

[42] M. Dutta, V. Nicolosi, A. Obratzova, A. Koos, A. Crossley, N. Grobert, Stable dispersions of nitrogen containing multi-walled carbon nanotubes, Mater. Express 1 (2011) 201-209.

[43] J.W. Jang, C.E. Lee, S.C. Lyu, T.J. Lee, C.J. Lee, Structural study of nitrogen doping effects in bamboo-shaped multiwalled carbon nanotubes, Appl. Phys. Lett. 84 (2004) 2877-2879.

[44] S. Maldonado, S. Morin, K.J. Stevenson, Structure, composition and chemical reactivity of carbon nanotubes by selective nitrogen doping, Carbon 44 (2006) 1429-1437.

[45] H. Liu, R. Zhang, R. Li, X. Sun, S. Desilets, H. Abou-Rachid, M. Jaidann, L.S. Lussier, Structural and morphological control of aligned nitrogen-doped carbon nanotubes, Carbon 48 (2010) 1498-1507.

[46] G. Liu, Q.D. Ling, Y.H. Teo, C.X. Zhu, D.S.H. Chan, K.G.Neoh, E.T. Kang, Electrical conductance tuning and bistable switching in poly(N-vinylcarbazole)- carbon nanotube composite films, ACS Nano 3 (2009) 1929-1937.

[46] S. ChandraKishore, A. Pandurangan, Facile synthesis of carbon nanotubes and their use in the fabrication of resistive switching memory device, RSC Adv. 4 (2014) 9905-9911.

[48] J.J. Yang, F. Miao, M.D. Pickett, D.A.A. Ohlberg, D.R. Stewart, C.N. Lau, R.S. Williams, The mechanism of electroforming of metal oxide memristive switches, Nanotechnology 20 (2009) 215201.

[49] J.J. Yang, M.D. Pickett, X. Li, D.A.A. Ohlberg, D.R. Stewart, R.S. Williams, Switching mechanism of metal/oxide/metal nanodevices, Nature Nanochnol. 3 (2008) 429-433.

[50] H.Y. Jeong, J.Y. Lee, S.Y. Choi, J.W. Kim, Microscopic origin of bipolar resistive switching of nanoscale titanium oxide thin films, Appl. Phys. Lett. 95 (2009) 162108.

[51] Y. Liu, L. Li, S. Wang, P. Gao, P. Zhou, J. Li, Z. Weng, L. Pan, J. Zhang, Subband transport mechanism and switching properties for resistive switching nonvolatile memories with structure of silver/aluminium oxide/p-type silicon, Appl. Phys. Lett. 106 (2015) 063506.

[52] S. Nigo, M. Kubota, Y. Harada, T. Hirayama, S. Kato, H. Kitazawa, G. Kido, Conduction band caused by oxygen vacancies in aluminium oxide for resistance random access memory, J. Appl. Phys. 112 (2012) 033711.

[53] W. Kim, S.I. Park, Z. Zhang, S. Wong, Current conduction mechanism of nitrogen-doped AlOx RRAM, IEEE Trans. Electron Dev. 61 (2014) 2158-2163.

a)

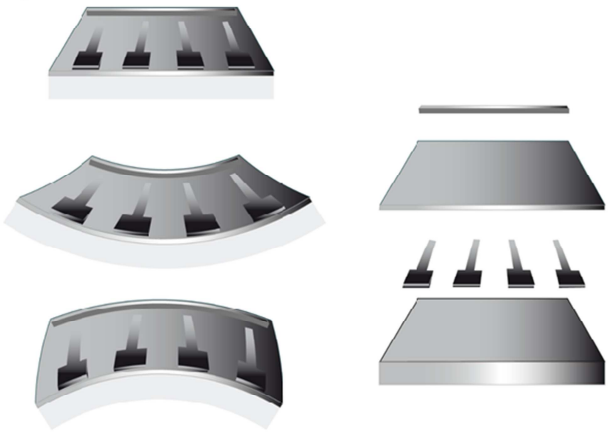

b)

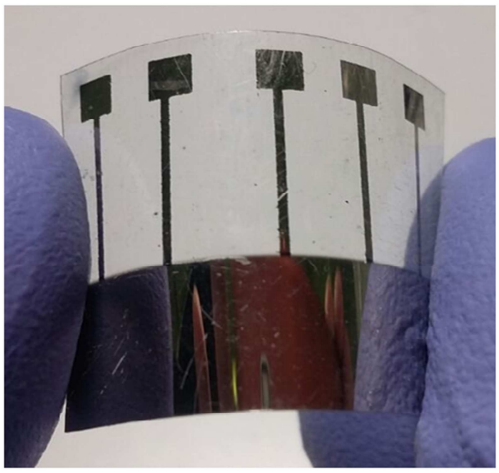

a)

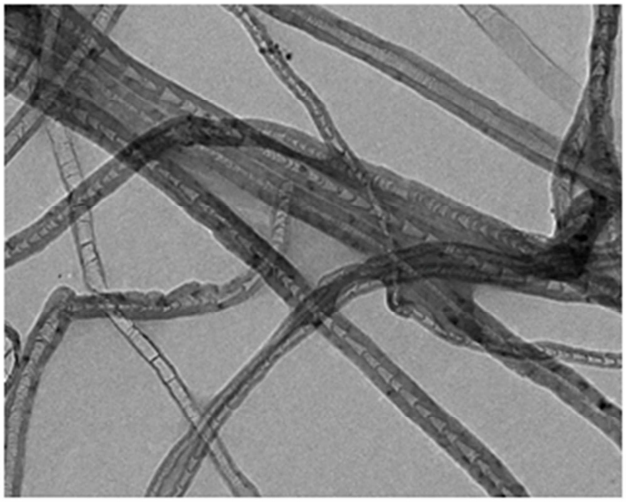

b)

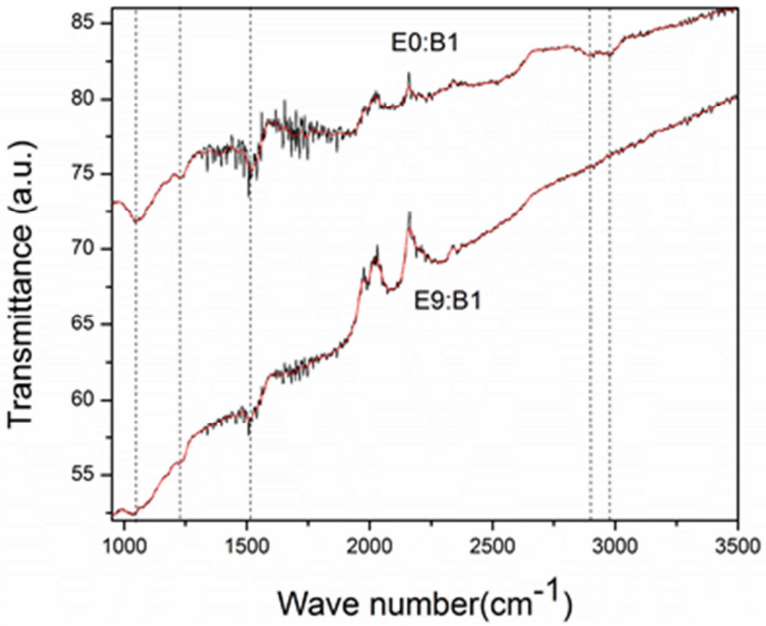
E0:B1
E9:B1
Transmittance (a.u.)
85
80
75
70
65
60
55
1000
1500
2000
2500
3000
3500
Wave number(cm-1)

c)

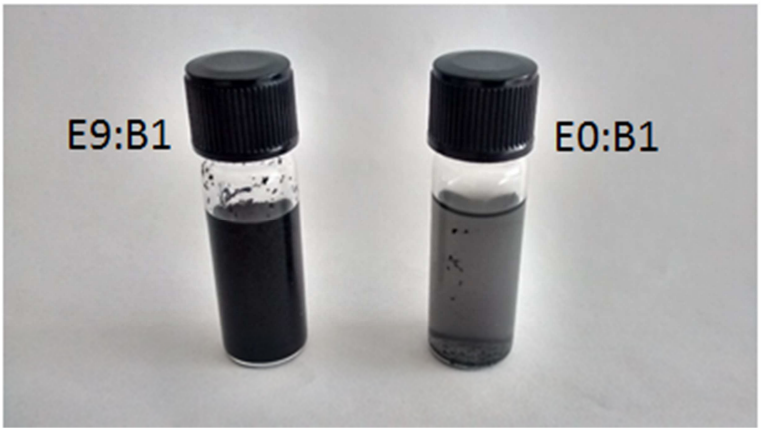
E9:B1
E0:B1

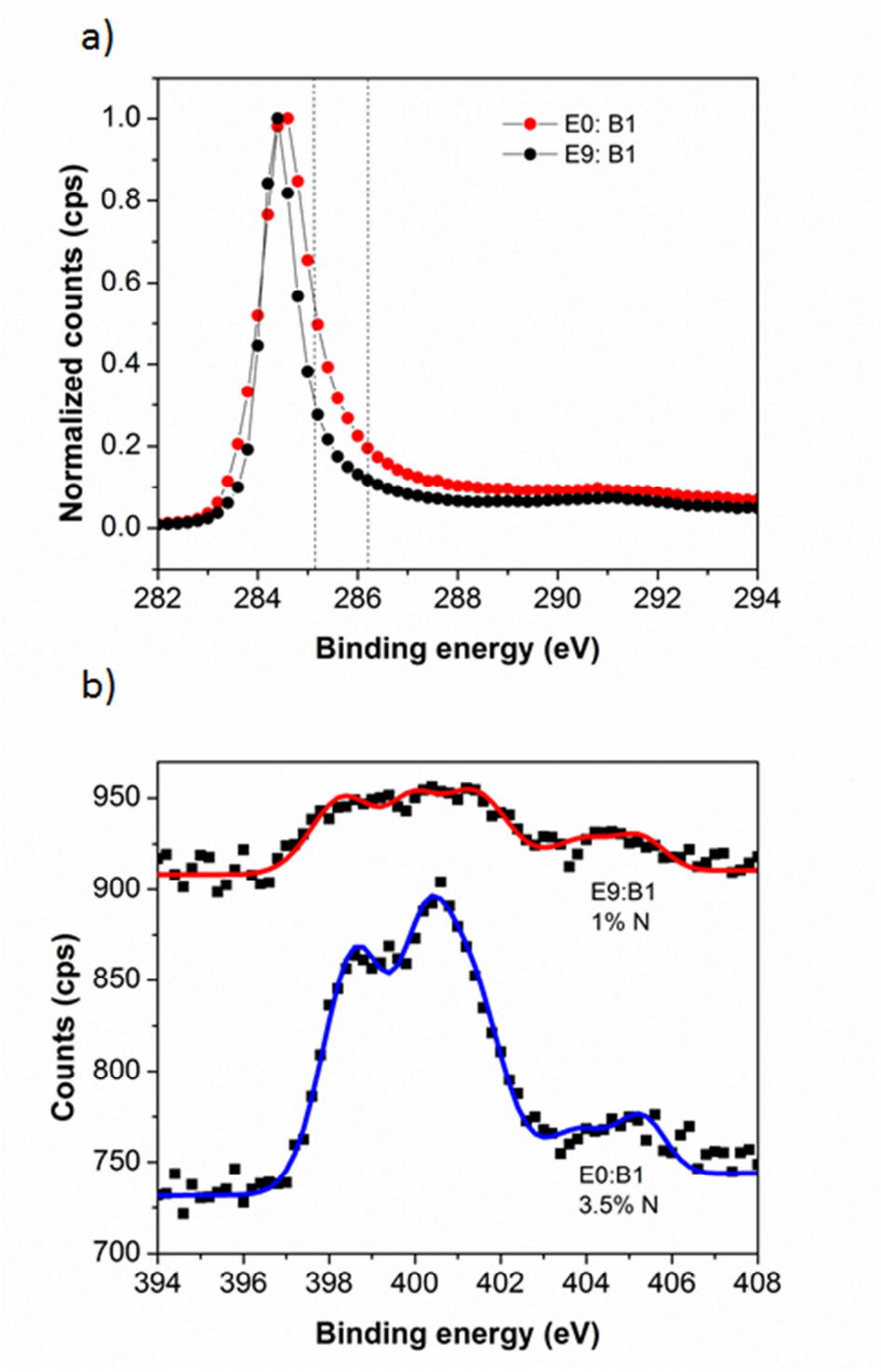
a)
Normalized counts (cps)
1.0
0.8
0.6
0.4
0.2
0.0
E0: B1
E9: B1
282
284
286
288
290
292
294
Binding energy (eV)
b)
Counts (cps)
950
900
850
800
750
700
E9:B1
1% N
E0:B1
3.5% N
394
396
398
400
402
404
406
408
Binding energy (eV)

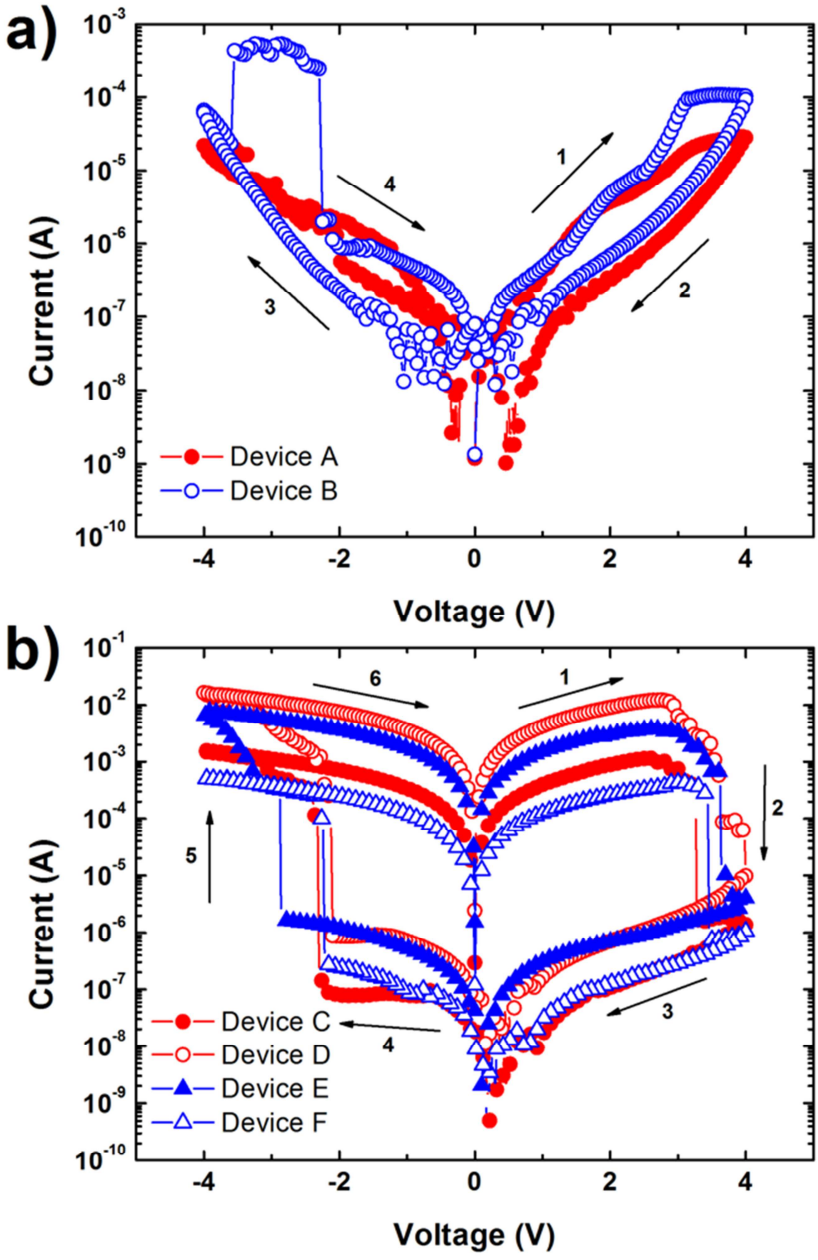
a)
Current (A)
Voltage (V)
Device A
Device B
1
2
3
4
b)
Current (A)
Voltage (V)
Device C
Device D
Device E
Device F
1
2
3
4
5
6

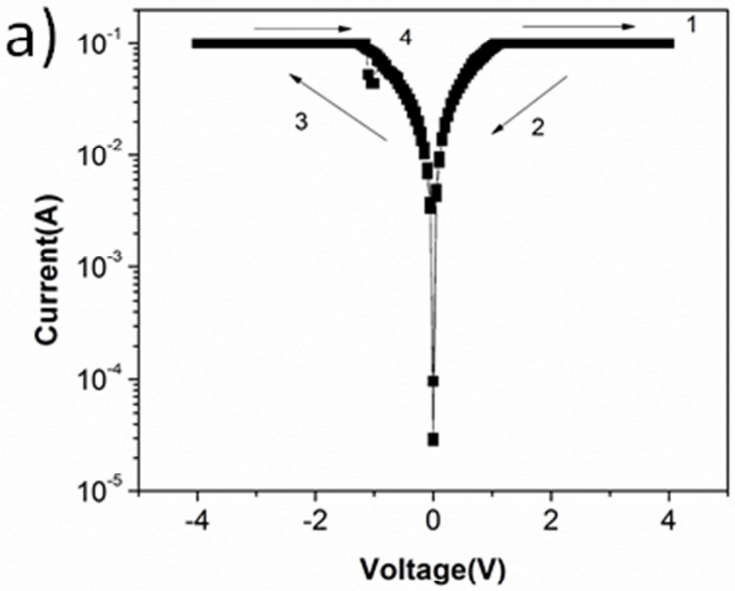
a)
Current(A)
Voltage(V)
1
2
3
4

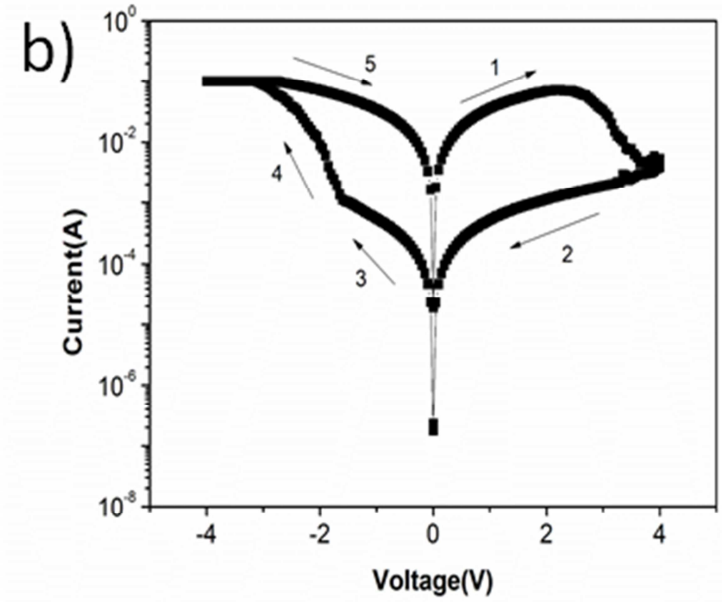
b)
Current(A)
Voltage(V)
1
2
3
4
5

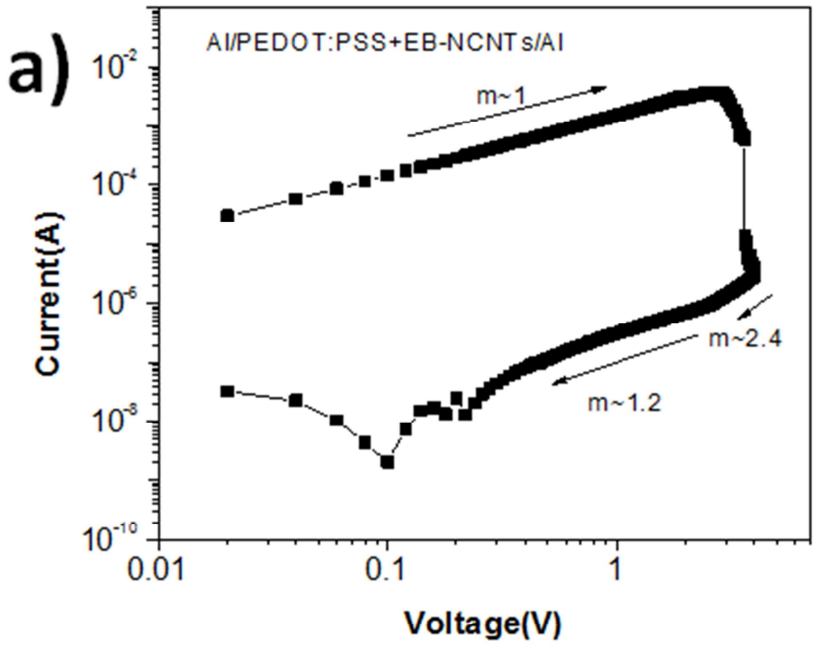
a)
Al/PEDOT:PSS+EB-NCNTs/Al
m~1
m~2.4
m~1.2
Current(A)
Voltage(V)
10^-2
10^-4
10^-6
10^-8
10^-10
0.01
0.1
1

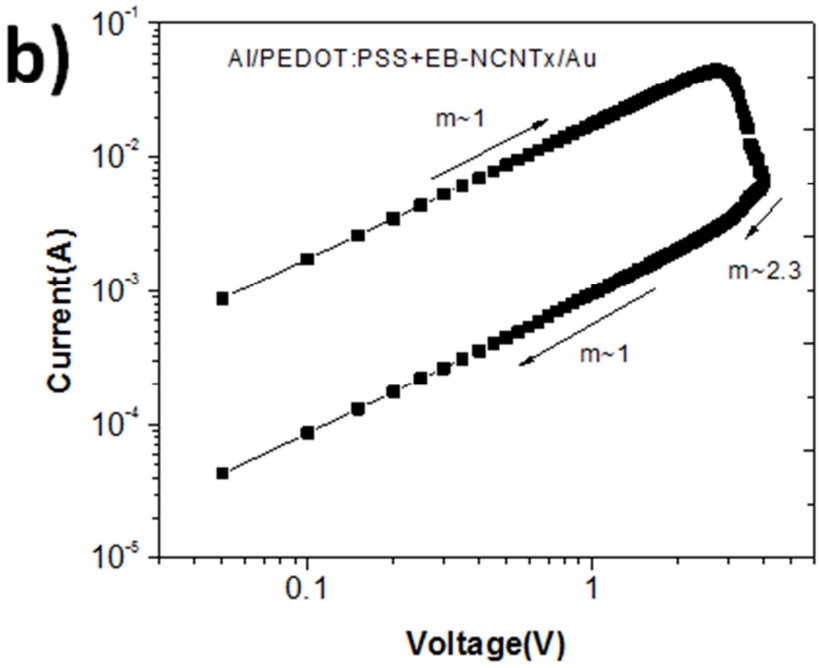
b)
Al/PEDOT:PSS+EB-NCNTx/Au
m~1
m~2.3
m~1
Current(A)
Voltage(V)
10^-1
10^-2
10^-3
10^-4
10^-5
0.1
1

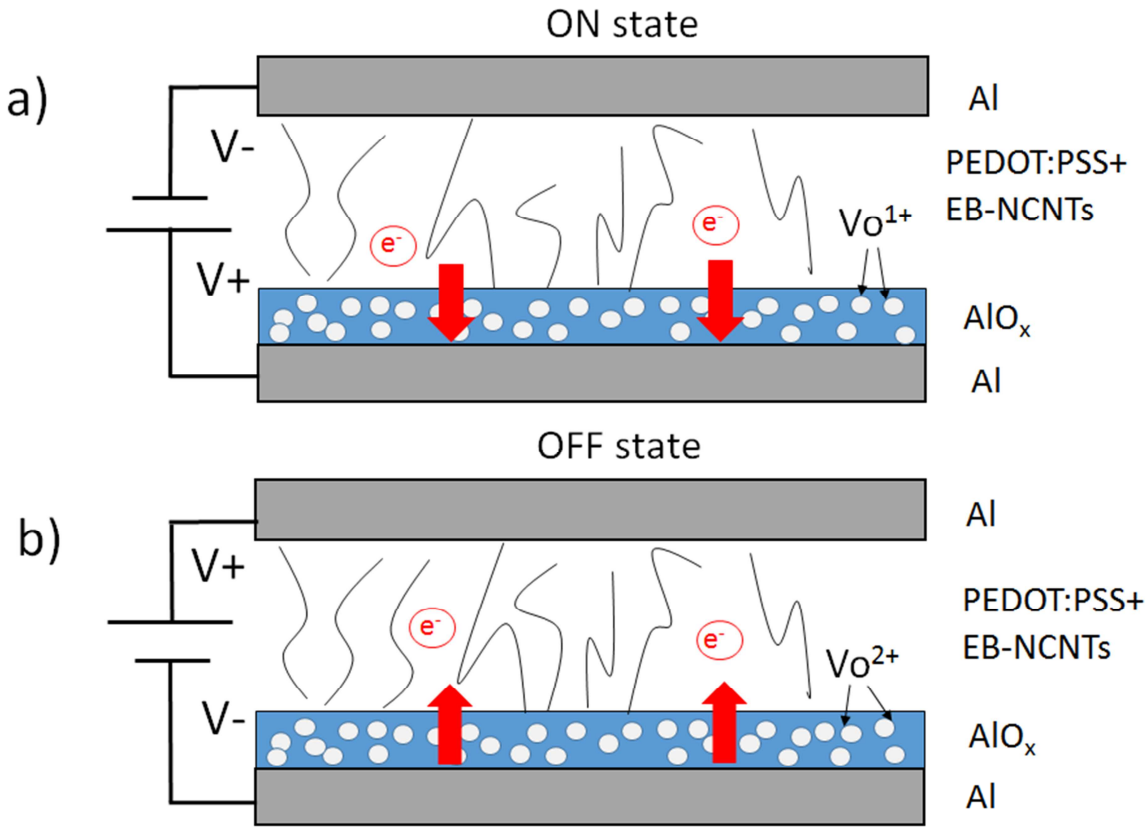

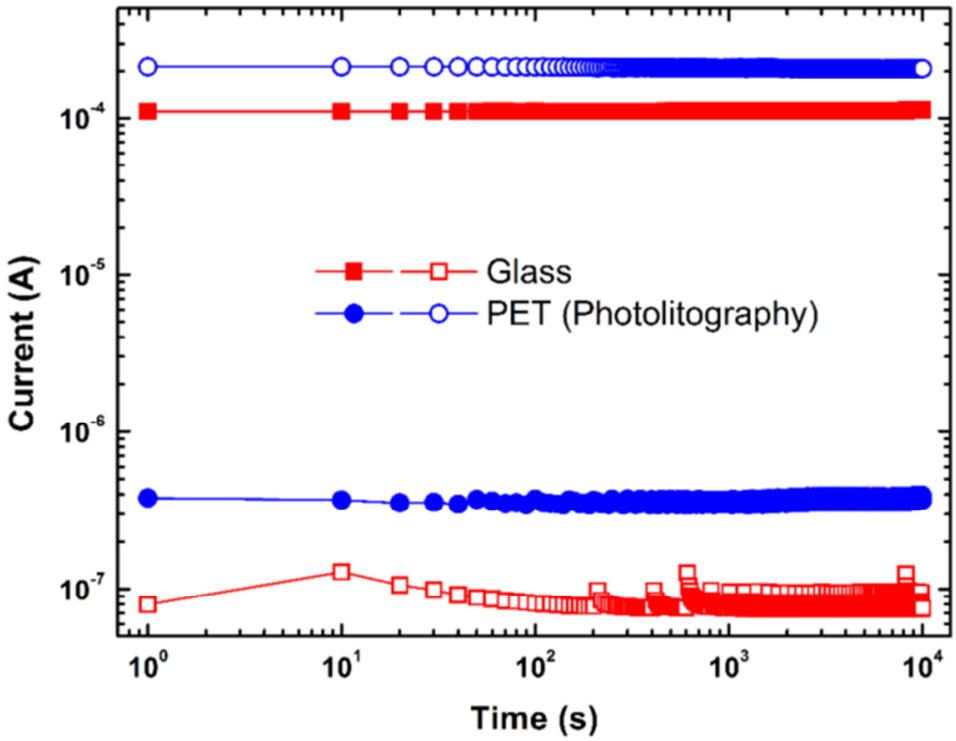

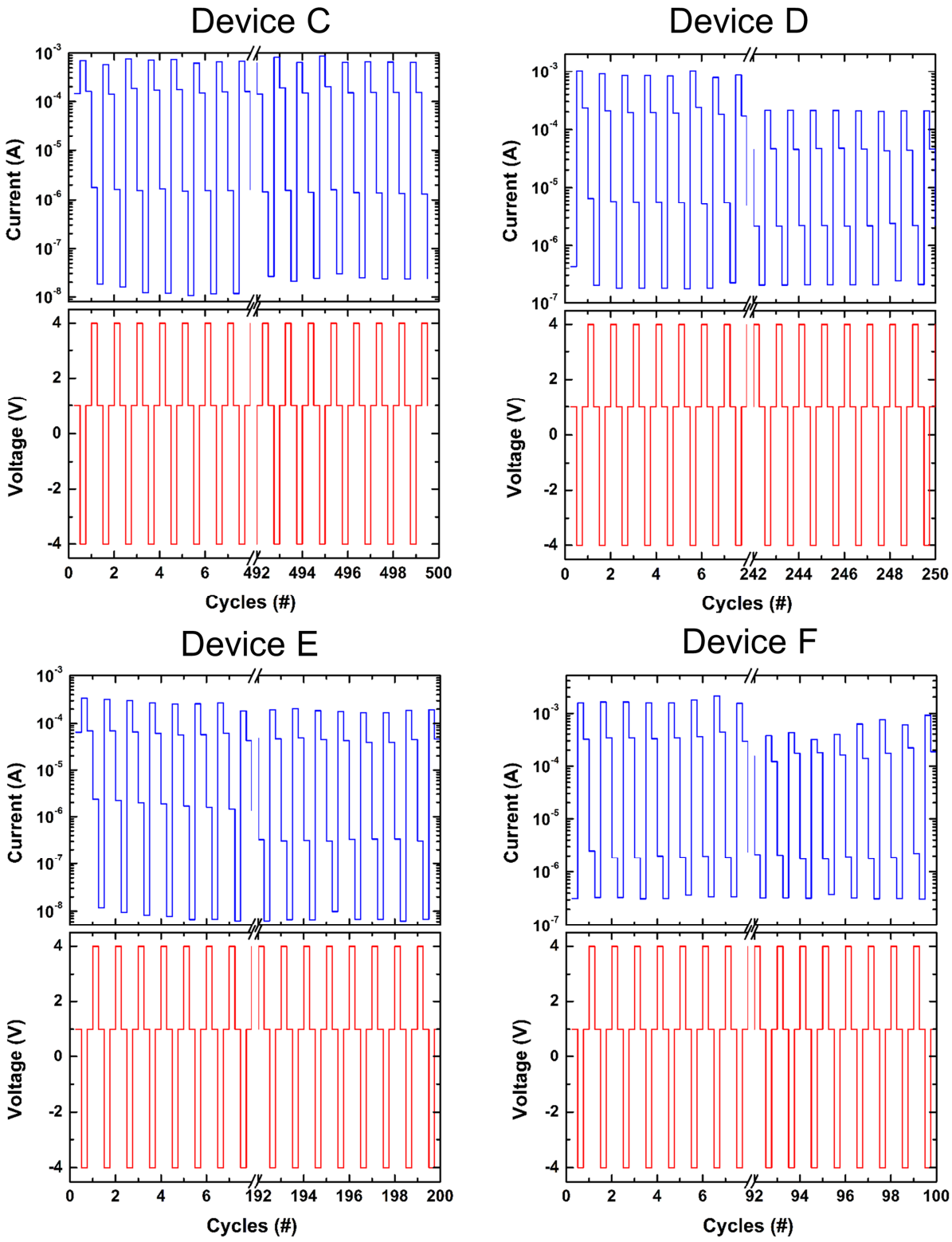
Device C
Device D
Device E
Device F
Current (A)
Voltage (V)
Cycles (#)

Highlights

Native AlOx layer on the bottom electrode is necessary to obtain resistive switching

Physical deformation on top electrode indicates creation of oxygen vacancies.

Functionalization on the NCNT surface improves device reliability

Low NCNT concentration (~0.002 wt%) in PEDOT:PSS is essential for resistive switching